**Research & Reviews: Journal of Material Sciences**
DOI: 10.4172/2321-6212.1000225

e-ISSN: 2321-6212
p-ISSN: 2347-2278

# Synthesis, Characterization and Effect of Increasing Nitrogen Concentration on the Growth of ZnO Nanoparticles

**Sukhpreet Singh*, Tushar Mahajan and Kiratbir Kaur**

Department of Nanotechnology, S.G.G.S.W.U, Fatehgarh Sahib, Punjab, India

## Research Article

Received: 07/06/2018
Accepted: 03/07/2018
Published: 13/07/2018

***For Correspondence**

Sukhpreet Singh, Department of Nanotechnology, S.G.G.S.W.U, Fatehgarh Sahib, Punjab, India, Tel: +919041788295.

**Email:** sukhpreetpb@gmail.com

**Keywords:** Zinc oxide, Nanoparticles

**ABSTRACT**

Highly crystalline ZnO nanoparticles were synthesized using a co-precipitation method by reaction of Zinc acetate with ammonium hydroxide in the presence of urea to obtain N-doped ZnO nanoparticles. X-ray diffraction studies showed the formation of crystalline hexagonal nitrogen incorporated ZnO. SEM result shows the morphology of the quasi-spherical particles with the average size of 90 nm. UV-Visible and Photoluminescence were carried out to check the luminescent behavior of the synthesized nanoparticles. FTIR studies were carried out to take information about different bonds. Our study showed that with the increase in the concentration of urea not only the Nitrogen gets doped into the ZnO nanoparticles but also it acts like a capping agent by decreasing the particle size with increase in concentration.

## INTRODUCTION

Nano science and nanotechnology have been making significant progress and their effect on every field has been truly acknowledged in the world. Nanotechnology which involves the manipulation of the matter at Nano and molecular scale perceived attention in miniaturization of semiconductors, optical and electronic devices [1,2]. Among the unique properties of nanomaterial, the movement of electrons and holes in semiconductor nanomaterial is primarily governed by the well-known quantum confinement, and the transport properties related to phonons and photons are largely affected by the size and geometry of the materials [3-6]. The specific surface area and surface-to-volume ratio increase drastically as the size of the material decreases [3,7]. Parameters such as size, shape, and surface characteristics can be varied to control their properties for different applications of interest [8].

Semiconductor Nano crystals (NCs) can be synthesized from a variety of different compounds. They are referred to as II-VI, III-V or IV-VI semiconductor Nano crystals, based on the periodic table groups into which these elements are formed. For example, silicon and germanium are group IV, InP, GaN, GaP, GaAs, GaP, and InAs are III-V, while those of CdS, CdSe, ZnO, ZnS, and CdTe are II-VI semiconductors.

Zinc oxide (ZnO) nanoparticles are a very interesting material because of their wonderful applications in the construction of electronic, optical, and acoustic devices [9]. ZnO is a semiconductor material with a direct wide band gap energy (3.37 eV) and a large exciton binding energy (60 meV) at room temperature [10]. Due to this Nanostructured ZnO finds applications in spintronics due to its ferromagnetic properties which in turn depend upon the grain boundaries in doped ZnO [11,12]. Due to their remarkable performance in electronics, optics, and photonics, ZnO NPs are attractive candidates for many applications such as UV lasers, light-emitting diodes, solar cells, Nano generators, gas sensors, photo-detectors, and photo catalysts [13-19].

Various methods for preparing ZnO nanoparticles have been investigated such as sol-gel process [20,21], chemical co-precipitation [22,23], chemical vapor deposition [24], thermal decomposition [25,26], hydrothermal synthesis [27], solid-state reaction [28], spray pyrolysis [29], and micro-emulsion precipitation [30-32]. These methods have allowed us to obtain various ZnO structures such as Nano spheres, Nano rods, Nanowires, and Nanotubes.

Among ZnO NP synthesis majority of the researchers have used sol gel method. Nano crystalline zinc oxide with different particle shapes and sizes was synthesized by hydrothermal method [33]. .Nano crystalline zinc oxide with zinc 2-ethylhexanoate (ZEH) and effect of ZEH concentration was studied [34]. Studies showed the use of cationic surfactant CTAB (cetyltrimethylammonium bromide) controls not only growth and nucleation of crystallites during synthesis, and also prevents the formation of agglomerates [35]. By using emulsion method role of surfactant Span 80 on ZnO NPs was studied [36]. Microcrystals of zinc oxide

**Research & Reviews: Journal of Material Sciences**
DOI: 10.4172/2321-6212.1000225
e-ISSN: 2321-6212
p-ISSN: 2347-2278

with various shapes (including forms approximating rice grains, nuts and rods) in the presence of sodium dodecyl sulfate (SDS) and triethanolamine (TEA) as cationic surfactant [37]. Thin layer of zinc oxide was prepared using pulsed laser deposition, under pressure effect of temperature on the structural and optical properties was determined [38]. Microwaves heating effect of precursors used on the morphology and aggregation of ZnO [39]. AAO (anodic aluminum oxide) assisted synthesis of ordered ZnO nanotubes was demonstrated [40]. By chemical synthesis pH affected the size and shape of the ZnO particles was demonstrated [41]. Hall effect on the synthesized Nano hetero-junction (p-ZnO/n-Si) which have wide range applications in, BJTs, MOSFETs and other electronic circuitry [42]. Three routes by emulsion, micro emulsion, and chemical precipitation with surfactant (cationic, anionic or non-ionic) was synthesized [43]. N-doped, P-type ZnO thin films have been grown by plasma-assisted metal-organic chemical vapor deposition method for the determination of donor/acceptor energy levels [44]. By the incorporation of dopants or formation of a composite with other materials, the photo catalytic properties of ZnO could be enhanced [45].

In our study, we synthesize highly crystalline ZnO nanoparticles using a co-precipitation method. Effect of nitrogen on the growth of particle size was examined. Different characterization tools such as X-ray diffraction, SEM, DLS, FTIR, UV-Visible and Photoluminescence were carried out to KNOW ABOUT particle size, morphology, different bond and the luminescent behavior of the synthesized nanoparticles. Studies showed the formation of crystalline hexagonal nitrogen incorporated ZnO with quasi-spherical particles with the average size of 90 nm was synthesized. Behind synthesis following reaction is carried out.

For preparing zinc oxide through chemical route, there are two phases which can be categorised as initial and dehydration phase.

Initial phase: Initially, zinc hydroxide was formed as given below:

$$Zn(NO_3)_2.\ 6H_2O+2NaOH=Zn(OH)_2\ (gel)+2NaNO_3+6H_2O \quad (1)$$

Dehydration Phase: The following reaction (2) took place in the dehydration phase:

$$Zn(OH)_2\ (gel)=ZnO\ (s)+H_2O \quad (2)$$

## EXPERIMENTAL SECTION

Zinc nitrate hexahydrate (Zn $(NO_3)26H_2O$) was procured from Sigma Aldrich and Sodium hydroxide (NaOH) and Urea (Nitrogen) ($CH_4N_2O$) were procured from HIMEDIA. All the chemicals were used in analytical grade and without further purification. Deionized water was used throughout the experiment.

ZnO nanoparticles were prepared by co-precipitation method. A volume of 50 ml of 0.1 M zinc nitrate hexahydrate precursor aqueous solution was prepared under vigorous stirring for 20 min. 25 ml aqueous solution of 0.2 M NaOH was added drop wise to 50 ml of zinc salt precursor solution under constant stirring and the reaction was continued for 40 min, yielding a white precipitate. Thereafter, the solution was allowed to settle for 3 h, the particle suspension was transferred to centrifuging tubes and subjected to centrifuging at 3000 rpm for 10 min. In each centrifugation, the reaction medium was changed using distilled water and ethanol and is repeated thrice. Then, the precipitates were dried at room temperature for overnight. In order to study the influence of Urea (Nitrogen) ($CH_4N_2O$) on the formation of ZnO nanoparticles, concentration of Urea (Nitrogen) ($CH_4N_2O$ was varied from 0.2,0.3 M, and 0.4 M. Effect on the particle size with the increase in concentration of nitrogen was examined. The crystal structure and phase analysis of the nanostructures were investigated using an X-ray diffractometer (Bruker Advance R8) in the angular range of 2q from 20 to 80°. Size determination was carried Dynamic Light scattering (Malvern S90). The surface morphological analysis of the nanoparticles was studied using FE-SEM (Merlin-Compact). Various bonds between undoped and doped nitrogen ZnO nanoparticles were examined by FTIR (Bruker ALPHA). UV-visible absorption spectra of all the samples were recorded using a UV-visible spectrophotometer (Schimadzu UV-2600). Photoluminescence emission spectrum was recorded at Photoluminescence (EdinburInstrumentsFLS 980) **(Figure 1)**.

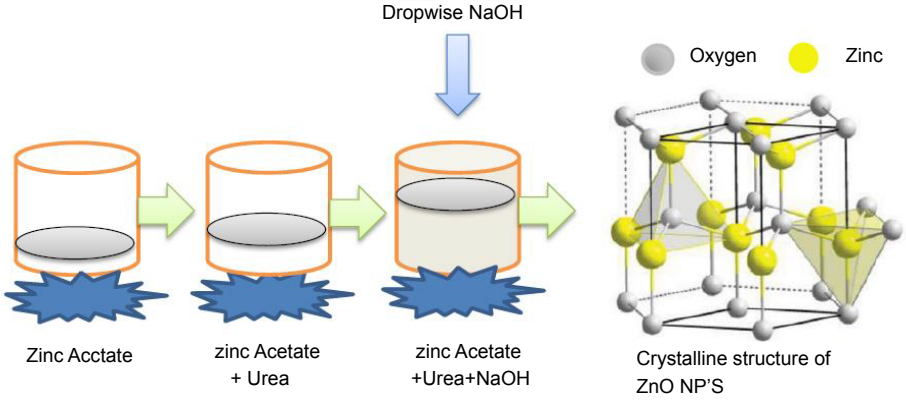


**Figure 1.** Synthesis of ZnO Nanoparticles.

Research & Reviews: Journal of Material Sciences
DOI: 10.4172/2321-6212.1000225
e-ISSN: 2321-6212
p-ISSN: 2347-2278

## RESULTS AND DISCUSSION

### Fourier Transform Infrared Spectroscopy

Fourier transform infrared spectroscopy gives the information about the functional group attached to the material. **Figure 2** Undoped ZnO where peak at 3390 $cm^{-1}$ shows absorption of Zn-O bonds. Peaks at 1391 and 1579 $cm^{-1}$ are asymmetric and symmetric stretching of Zinc Carboxylic due to C=O, O-H bending vibration. Peak at 882 $cm^{-1}$ shows carboxylic and hydroxyl impurities. Peak at 676 $cm^{-1}$ show Zn-O bond peak. **Figure 3**, 0.2 M Nitrogen Doped ZnO. In this peaks at 3855 and 3747 $cm^{-1}$ shows hydroxyl due to O-H stretching vibration. Peak at 2969 $cm^{-1}$ show C-H stretching vibration of alkane group. Peaks at 1744 and 1522 $cm^{-1}$ show asymmetric and symmetric stretching of Zinc Carboxylic due to C=O, O-H bending vibration. Peak at 1052 $cm^{-1}$ shows carboxylic and hydroxyl impurities. The FTIR spectra did not present any of the characteristic bands of the urea, which is presented at 3210 $cm^{-1}$. **Figure 4** peaks at 3742 $cm^{-1}$ shows hydroxyl due to O-H stretching vibration. Peaks at 1393, 1522 and 1694 $cm^{-1}$ show asymmetric and symmetric stretching of Zinc Carboxylic due to C=O, O-H bending vibration. Peak at 896 $cm^{-1}$ shows carboxylic and hydroxyl impurities. Peak at 669 $cm^{-1}$ show Zn-O bond peak. **Figure 5**, peak at 3740 $cm^{-1}$ shows hydroxyl due to O-H stretching vibration. Peaks at 1396, 1541 and 1638 $cm^{-1}$ show asymmetric and symmetric stretching of Zinc Carboxylic due to C=O, O-H bending vibration. Peak at 911 $cm^{-1}$ shows carboxylic and hydroxyl impurities.

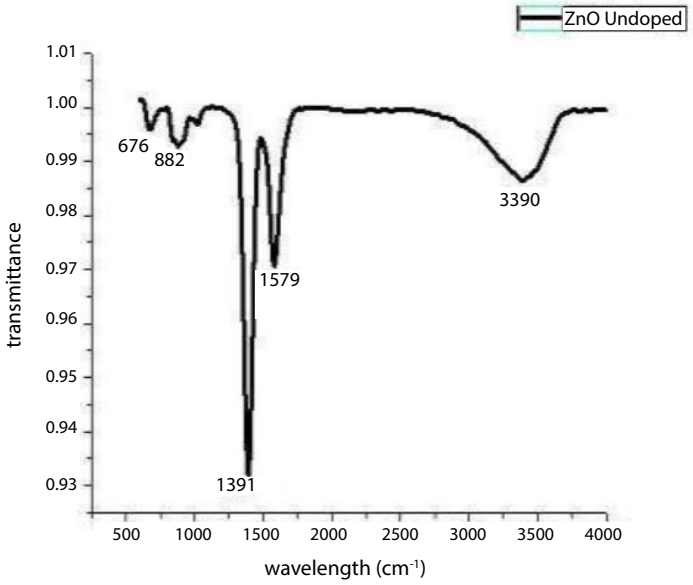


**Figure 2.** Undoped ZnO

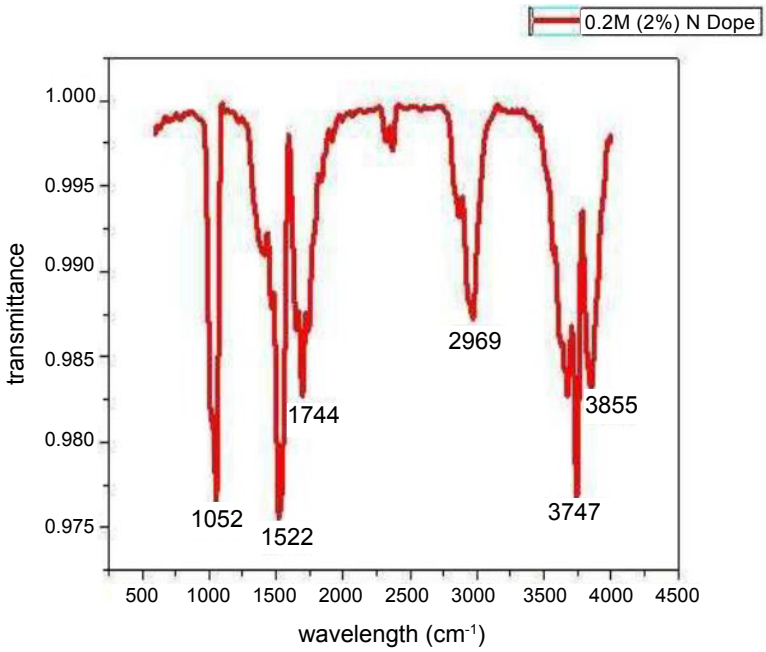


**Figure 3.** 0.2 M Doped ZnO.

Research & Reviews: Journal of Material Sciences
DOI: 10.4172/2321-6212.1000225
e-ISSN: 2321-6212
p-ISSN: 2347-2278

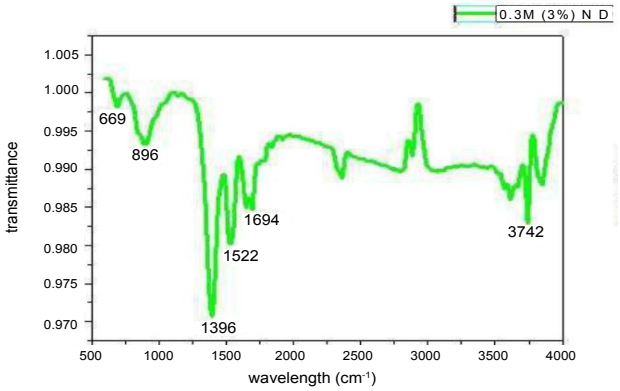


**Figure 4.** 0.3 M Doped ZnO.

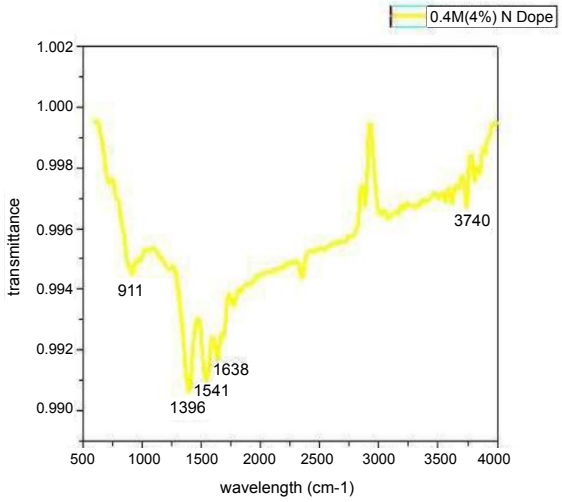


**Figure 5.** 0.4 M Doped ZnO.

### DLS and Zeta-Potential Analysis

Dynamic light scattering (DLS) which is based on the laser diffraction method with multiple scattering techniques was employed to study the average particle size of Zinc Oxide nanoparticles. It was based on Mie-scattering theory.. The size of the Undoped ZnO nanoparticles is 349.1 nm in **Figure 6** and size of the Doped ZnO nanoparticles with the doped Nitrogen 0.2 M is 325.2 nm in **Figure 7**, 0.3 M is 127.1 nm in the **Figure 8** and 0.4 M is 96.77 nm in the **Figure 9**.

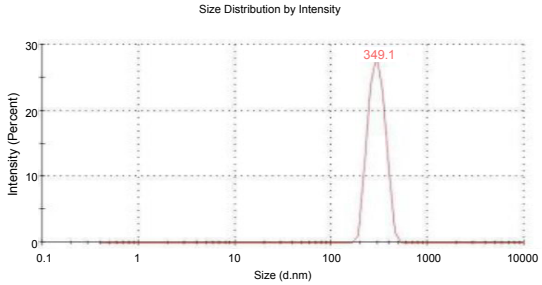


**Figure 6.** Undoped ZnO.

Research & Reviews: Journal of Material Sciences
DOI: 10.4172/2321-6212.1000225
e-ISSN: 2321-6212
p-ISSN: 2347-2278

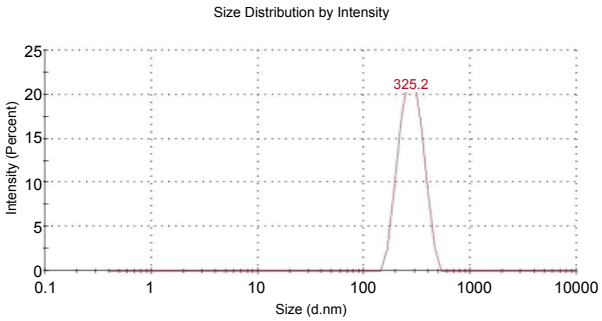


**Figure 7.** 0.2 M Doped ZnO.

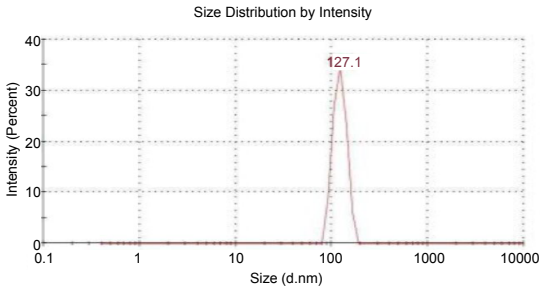


**Figure 8.** 0.3 M Doped ZnO.

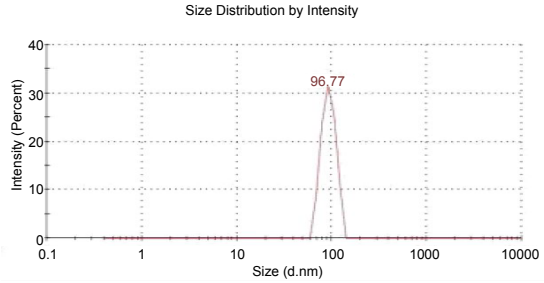


**Figure 9.** 0.4 M Doped ZnO.

### UV-Visible Spectroscopy

A UV-Visible spectrum shows the dependence of absorption coefficients on the photon energy for the ZnO nanoparticles. It is clear from this figure that the absorption coefficients obeys the direct equation better than the indirect equation. The optical direct band gap calculated from the formula hv=1240/ƛ is 3.31 eV. These results clearly indicate that increase in nitrogen concentration causes blue shift in absorption spectra. This may be caused by the variation in size of the particles with nitrogen concentration. As the nitrogen concentration increases from 0.2 M to 0.4 M, there is an increase in band gap. This also shows that increasing the concentration up to 1 M allows us to get more band gap and enhanced luminescent

As observed in the UV-Vis spectra Nitrogen Doped ZnO show blue shift due to quantum confinement. ZnO Undoped is observed at 371.3 nm in the UV-Vis region. Now, with the doping of Nitrogen peak is observed blue shift due to quantum confinement (**Figure 10**).

Peak is observed at 0.2 M Nitrogen Doped is 369.1 nm in **Figure 11** and band gap is 3.35 eV.

Peak is observed at 0.3 M Nitrogen Doped is 367.4 nm in **Figure 12** and band gap is 3.37 eV.

Peak is observed at 0.4 M Nitrogen Doped is 364.7 nm in **Figure 13** and band gap is 3.40 eV.

Research & Reviews: Journal of Material Sciences
DOI: 10.4172/2321-6212.1000225
e-ISSN: 2321-6212
p-ISSN: 2347-2278

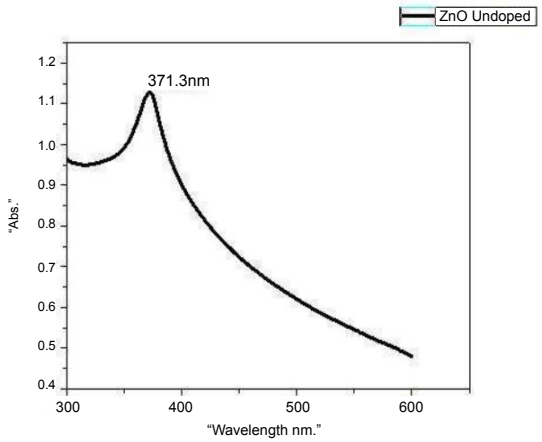


**Figure 10.** Undoped ZnO.

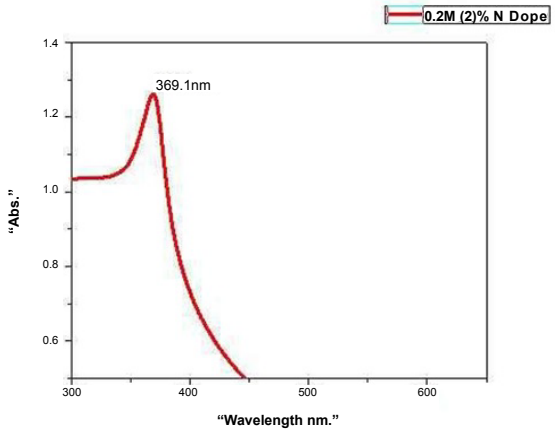


**Figure 11.** 0.2 M Doped ZnO.

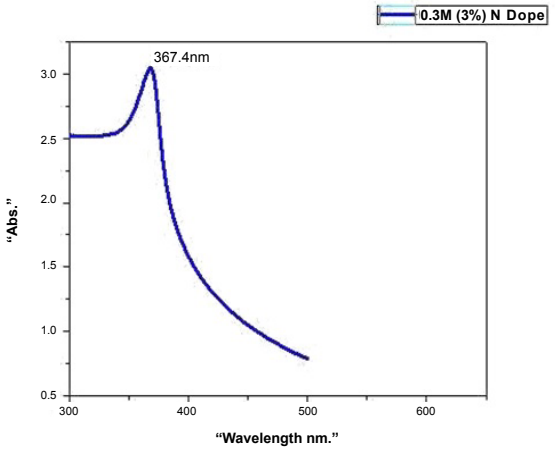


**Figure 12.** 0.3 M Doped ZnO.

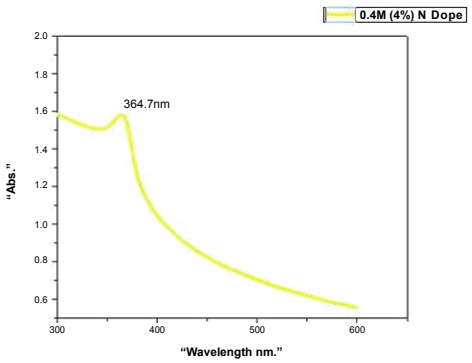


**Figure 13.** 0.4 M Doped ZnO.

Research & Reviews: Journal of Material Sciences
DOI: 10.4172/2321-6212.1000225
e-ISSN: 2321-6212
p-ISSN: 2347-2278

### X-Ray Diffraction

**Figure 14** represents the X-Ray diffraction pattern of ZnO nanopowder. A definite line broadening of the XRD peaks indicates that the prepared material consist of particles in nanoscale range. From this XRD patterns analysis, we determined peak intensity, position and width, full-width at half-maximum (FWHM) data. The diffraction peaks located at 31.86°, 34.44°, 36.31°, 47.65°, 56.70°, 62.87°, 66.46°, 68.04°, and 69.19° These lines were indexed respectively as (100), (002), (101), (102), (110), (103), (200), (112) and (201) and correspond to hexagonal wurtzite phase of ZnO have been keenly indexed a have been keenly indexed as hexagonal wurtzite phase of ZnO with Lattice constants $a=b=0.324$ nm and $c=0.521$ nm (JPCDS card number: 36-1451) and further it also confirms the synthesized nanopowder was free of impurities as it does not contain any characteristics XRD peaks other than ZnO peaks. The synthesized ZnO nanoparticle diameter was calculated using Debye-Scherrer formula

$$d=0.89\lambda/\beta \cos\theta,$$

Where 0.89 is Scherrer's constant, $\lambda$ is the wavelength of X-Rays, $\theta$ is the Bragg diffraction angle, and $\beta$ is the full width at half-maximum (FWHM) of the diffraction peak corresponding to plane (101). The average particle size of the sample was found to be 350 nm which is derived from the FWHM of more intense peak corresponding to (101) planes located at 36.31° using Scherrer's formula.

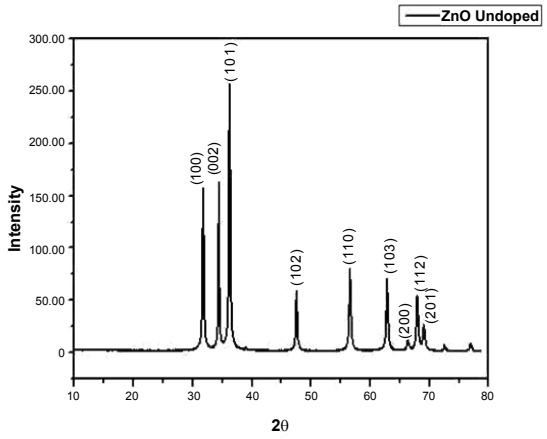


**Figure 14.** X-Ray Diffraction pattern of ZnO Undoped.

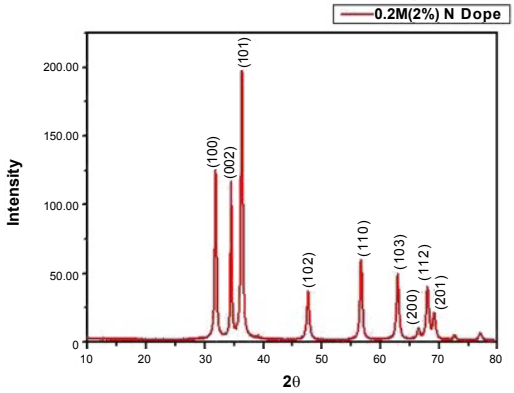


**Figure 15.** X-Ray Diffraction pattern of Nitrogen Doped ZnO.

**Figure 15** represents the X-Ray diffraction pattern of ZnO nanopowder. A definite line broadening of the XRD peaks indicates that the prepared material consist of particles in nanoscale range. From this XRD patterns analysis, we determined peak intensity, position and width, full-width at half-maximum (FWHM) data. The diffraction peaks located at 31.85°, 34.46°, 36.28°, 47.56°, 56.66°, 62.91°, 66.41°, 68.00°, and 69.16° These lines were indexed respectively as (100), (002), (101), (102), (110), (103), (200), (112) and (201) and correspond to hexagonal wurtzite phase of N Doped ZnO have been keenly indexed a have been keenly indexed as hexagonal wurtzite phase of N Doped ZnO with Lattice constants $a=b=0.324$ nm and $c=0.521$ nm (JPCDS card number: 36-1451) and further it also confirms the synthesized nanopowder was free of impurities as it does not contain any characteristics XRD peaks other than N Doped ZnO peaks. The synthesized N Doped ZnO nanoparticle diameter was calculated using Debye-Scherrer formula. No additional peak due to nitrogen was observed in any of the spectra and hence the occurrence of residual nitrogen or compound/complex of nitrogen, is also ruled out for prepared N Doped ZnO materials. In this context, it is well established that the lattice distortion due to the defects (vacancies, interstitials, substitutions, local structure transformations etc.) may cause the shift in XRD peak position depending on the type of strain in the crystal i.e., tensile or compressive strain, the peak position shifts respectively towards higher or lower angle. Since the ionic radii of N ($r_N^{2+}$=1.46 Å) is greater than that

e-ISSN: 2321-6212
p-ISSN: 2347-2278

for O ($r_O^{2+}$=1.38 Å), N substituting O in ZnO lattice may result in tensile strain along with the expansion of crystallite size. Thus, we conclude that N Doping into ZnO lattice is evident through peak position shift towards higher angle, however, the expansion of ZnO lattice due to N Doping does not increase after 0.2 M (2%) doping concentration. Similar to the shifting in (101) peak position, change in broadening of this peak may also be noticed in **Figure 15**. Since the peak broadening reflects the alteration in crystallite size, it appears that crystallite size also changes with N Doping. However, the change in lattice constant is observed from 0.2 M (2%) N Doping and it does not change afterwards in 0.3 M (3%) and 0.4 M (4%)., Where 0.89 is Scherrer's constant, $\lambda$ is the wavelength of X-Rays, $\theta$ is the Bragg diffraction angle, and $\beta$ is the full width at half-maximum (FWHM) of the diffraction peak corresponding to plane (101). The average particle size of the sample was found to be 90 nm which is derived from the FWHM of more intense peak corresponding to (101) planes located at 36.28° using Scherrer's formula.

### Scanning Electron Microscopy

Morphology and particle size determination of undoped and nitrogen doped ZnO nanostructures was studied. **Figure 16** shows that the round and spherical shaped nanoparticles were synthesized. The average size of the Nitrogen doped ZnO is found to be 90 nm while for the undoped it is 350 nm **(Figure 17)**. Highly crystalline nanoparticle's are formed and are parallel with the XRD studies.

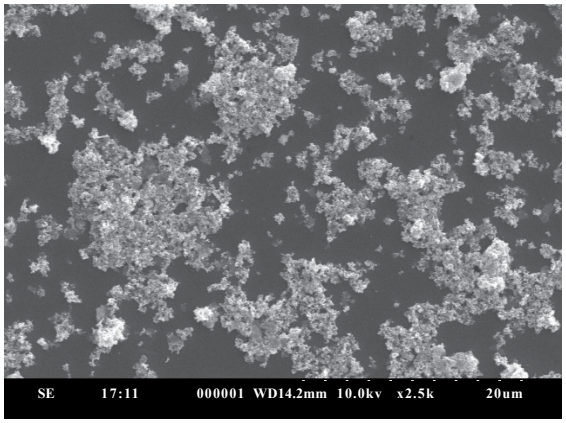


**Figure 16.** Scanning Electron Microscopy of ZnO Doped.

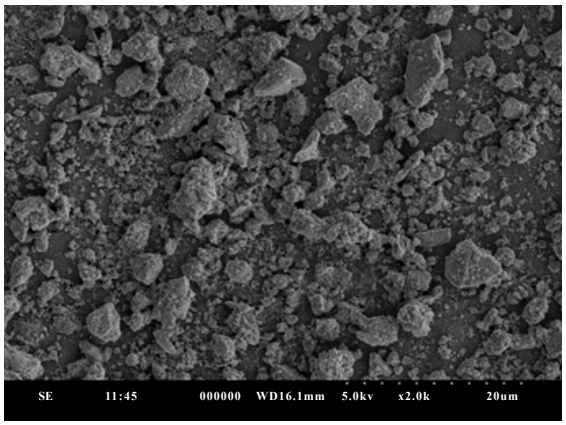


**Figure 17.** Scanning Electron Microscopy of Nitrogen Undoped ZnO.

### Photoluminescence

Photoluminescence (PL), properties of ZnO nanoparticle, is interesting as it provide valuable information on the purity and quality of the material. **Figures 18 and 19** shows the room temperature (RT) Photoluminescence spectra of the ZnO Undoped and Nitrogen Doped nanoparticles prepared from the Zinc Nitrate in the wavelength range 450-700 nm. **Figure 18** ZnO shows the emission spectrum sample, under the excitation of 450 nm. In the spectrum, there are four emission bands. The emission band ZnO Undoped in the visible region can be observed with a peak at 474 nm, 530 nm, 556 nm and 620 nm. Photoluminescence of ZnO Undoped nanoparticles at range 474 nm (2.61 eV) emit light in blue region is because of intrinsic defects such as oxygen and zinc interstitials, 530 nm (2.33 eV) and 556 nm (2.23 eV) emit light in green region which is caused by impurities, a structural defects in the crystal such as oxygen vacancies, zinc interstitials, etc and 620 nm (1.99 eV) emit light in red region due to oxygen and zinc anti-sites. **Figure 19** Photoluminescence of Nitrogen Doped ZnO shows the emission spectrum sample, under the excitation of nm. In the spectrum, there are four emission bands. The emission band of Nitrogen Doped ZnO in the visible region can be observed with a peak at 495 nm, 551 nm, 575 nm and 660 nm. Photoluminescence of Nitrogen Doped ZnO nanoparticles at range 495 nm (2.50 eV) and 551 nm (2.25 eV) emit light in green region which is caused by impurities, a structural defects in the crystal such as oxygen vacancies, zinc interstitials, etc, 575 nm (2.15 eV) emit light in yellow region and 660 nm (1.87 eV) emit

e-ISSN: 2321-6212
p-ISSN: 2347-2278

light in red region due to oxygen and zinc anti-sites. The green band emission corresponds to the singly ionized oxygen vacancy in ZnO in the bulk of nanoparticles and excess oxygen on the surface, which might be in the form of $OH^-$ ions and results from the recombination of photo-generated hole with single ionized charge state of this defect. The weak green emission also implies that there are few surface defects in ZnO nanoparticles.

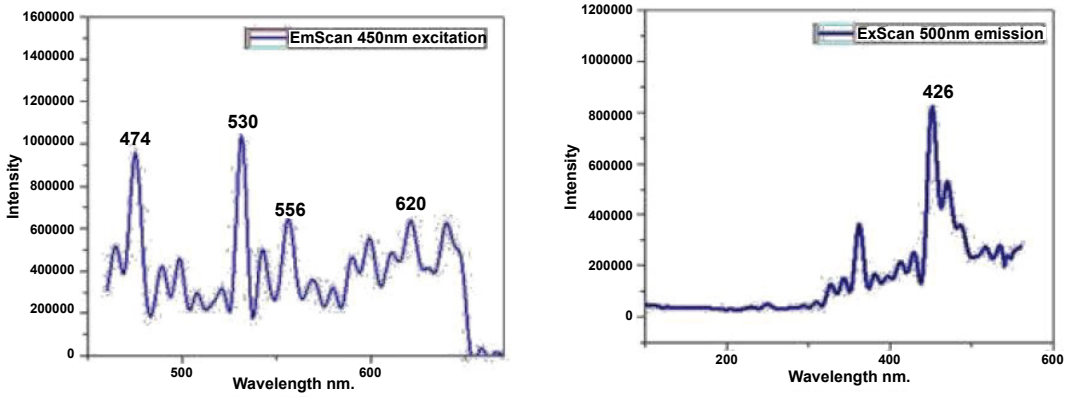


**Figure 18.** Photoluminescence of Undoped ZnO.

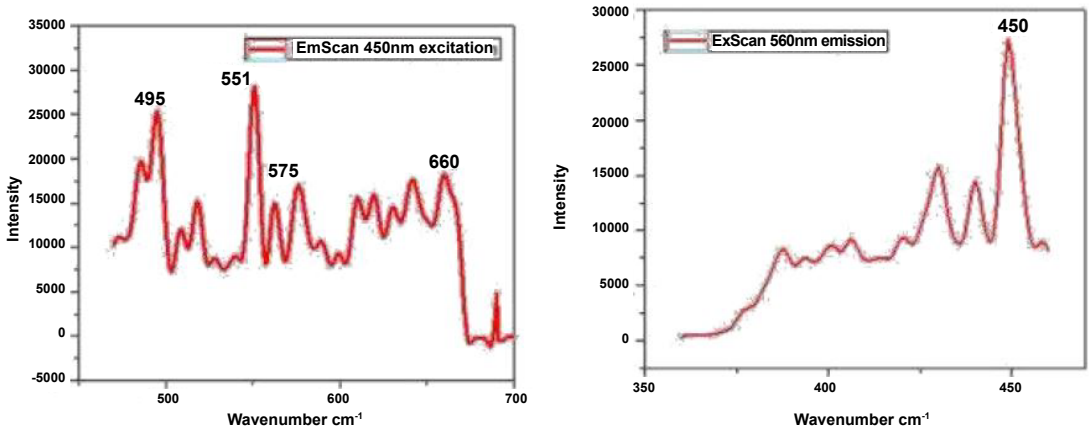


**Figure 19.** Photoluminescence of Nitrogen doped ZnO.

### Optimization and Size Determination Calibrations

By different characterizations and size determination tools, it is crystal clear that with the increase in concentration of corresponding the size of the ZnO nanoparticles decreases. So we have demonstrated a calibration curve for the synthesis procedure to find out the least minimum size of the ZnO nanoparticles with the effect of increase in concentration of nitrogen. In fig represents the particle size w.r.t. concentration with 0.2, 0.3, 0.4 doped nitrogen concentrations 325,137,96 nm size is obtained and the synthesis curve follows regression to be $R^2$=0.98 with particle to size determination with following equation y=17.514x-1.787

From this, it can be said that with the addition of 1 M nitrogen concentration we can get the 17 nm of the synthesized particles according to our purposed synthesized method.

## CONCLUSION

Highly crystalline ZnO nanoparticles were synthesized by co-precipitation method. In this work, attempts were made to tune the size of ZnO nanoparticles by controlling the growth parameters such as concentration of doped nitrogen. The XRD analysis of the samples confirmed its hexagonal wurtize phase. FE-SEM micrographs showed the morphology of nanoparticles as quasi-spherical with increase in concentration of the doped nitrogen decrease in the size is observed. The size of ZnO Undoped and Doped nanoparticles analyzed by Dynamic light scattering (DLS) is found to be in the range of 50-300 nm. Due to quantum confinement blue shift is observed in bulk UV-Vis spectra studies is observed at 374.5 nm optical energy gap determined by applying Tauc's equation is approximately equal to 3.31 eV. FTIR spectroscopy shows an increased carboxylate and hydroxyl concentration in samples of smaller size, indicating that they are probably near-surface impurities. It is believed that these surface carboxylate and hydroxyl impurities serve as primary non-radiative recombination centers during the relaxation processes

e-ISSN: 2321-6212
p-ISSN: 2347-2278

of photo-excited valence electrons in our samples. Different dopants and core shell nanoparticles can be further employs to enhance the properties of the synthesized nanomaterials.

## REFERENCES

1. Alivisatos AP. Perspectives on the Physical Chemistry of Semiconductor Nanocrystals. J Phys Chem 1996;100:13226-13239.
2. Stroscio JA and Eigler DM. Atomic and Molecular Manipulation with the Scanning Tunneling Microscope. Science 1991;254:1319-1326.
3. Burda C, et al. Chemistry and properties of nanocrystals of different shapes. Chem Rev 2005;105:1025-1102.
4. Murray CB, et al. Synthesis and characterization of monodisperse nanocrystals and close-packed nanocrystal assemblies. Annu Rev Mater Sci 2000;30:545-610.
5. Chen X, et al. Doped semiconductor nanomaterials. J Nanosci Nanotechnol 2005;5:1408-1420.
6. Li J and Zhang JZ. Optical properties and applications of hybrid semiconductor nanomaterials. Coordin Chem Rev 2009;253:3015-3041.
7. AQMD. Smog and Health. The south coast air quality management district 1996.
8. Sheethaler R. Synthesis report on health costs due to road traffic-related air pollution-an impact assessment project Austria, France and Switzerland. WHO Regional office for Europe.
9. Qian HS, et al. Growth of ZnO crystals with branched spindles and prismatic whiskers from $Zn_3(OH)_2V_2O_7H_2O$ nano sheets by a hydrothermal route. Crystal Growth Design 2005;5:935-939.
10. Lu F, et al. ZnO hierarchical micro/ nanoarchitectures: solvothermal synthesis and structurally enhanced photocatalytic performance. Adv Func Mater 2008;18:1047-1056.
11. Straumal BB, et al. Grain boundary layers in nanocrystalline ferromagnetic zinc oxide. JETP Lett 2010;92:396-400.
12. Straumal BB, et al. Amorphous interlayers between crystalline grains in ferromagnetic ZnO films Mater Lett 2012;71:21-24.
13. Chu S, et al. Electrically pumped waveguide lasing from ZnO nanowires. Nature Nanotechnol 2011;6:506-510.
14. Na JH, et al. Hybrid pn junction light-emitting diodes based on sputtered ZnO and organic semiconductors. Appl Phys Lett 2009;95:25.
15. Sudhagar P, et al. Facile synthesis of highly branched jacks-like ZnO nanorods and their applications in dye-sensitized solar cells. Mater Res Bull 2011;46:1473-1479.
16. Wang ZL, et al. Lateral nanowire/ nanobelt based nanogenerators, piezotronics and piezophototronics. Mater Sci Eng R 2010;70:320-329.
17. Xu J, et al. Studies on alcohol sensing mechanism of ZnO based gas sensors. Sensors Actuators B 2008;132:334-339.
18. Lu CY, et al. Ultraviolet photodetectors with ZnO nanowires prepared on ZnO:Ga/glass templates. Appl Phys Lett 2006;89:153101.
19. Cho S, et al. Large-scale fabrication of sub-20-nm-diameter ZnO nanorod arrays at room temperature and their photocatalytic activity. J Phys Chem C 2009;113:10452-10458.
20. Khrenov V, et al. Surface functionalized ZnO particles designed for the use in transparent nanocomposites. Macromolecular Chem Phys 2005;206:95-101.
21. Toutorski IA, et al. Mechanical properties and structure of zinc-containing latex-silicate composites. J Sol-Gel Sci Technol 2003;26:505-509.
22. Wang L and Muhammed M. Synthesis of zinc oxide nanoparticles with controlled morphology. J Mater Chem 1999;9:2871-2878.
23. Fernandez JF, et al. Controlled precipitation methods: formation mechanism of ZnO nanoparticles. J Eur Ceram Soc 2001;21:925-930.
24. Purica M, et al. Optical and structural investigation of ZnO thin films prepared by chemical vapor deposition (CVD). Thin Solid Films 2002;403-404:485-488.
25. Audebrand N, et al. X-ray diffraction study of the early stages of the growth of nanoscale zinc oxide crystallites obtained from thermal decomposition of four precursors. General concepts on precursor-dependent microstructural properties. Chem Mater 1998;10:2450-2461.
26. Yang Y, et al. Size control of ZnO nanoparticles via thermal decomposition of zinc acetate coated on organic additives. J Crystal Growth 2004;263:447-453.

e-ISSN: 2321-6212
p-ISSN: 2347-2278

27. Lu CH and Yeh CH. Influence of hydrothermal conditions on the morphology and particle size of zinc oxide powder. Ceram Int 2000;26:351-357.

28. Zhu Y and Zhou Y. Preparation of pure ZnO nanoparticles by a simple solid-state reaction method. Appl Phys A: Mater Sci Process 2008;92:275-278.

29. Tani T, et al. Homogeneous ZnO nanoparticles by flame spray pyrolysis. J Nanoparticle Res 2002;4:337-343.

30. Hingorani S, et al. Microemulsion mediated synthesis of zinc-oxide nanoparticles for varistor studies. Mater Res Bull 1993;28:1303-1310.

31. Hingorani S, et al. Effect of process variables on the grain growth and microstructure of ZnO-$Bi_2O_3$ varistors and their nanosize ZnO precursors. J Mater Res 1995;10:461-467.

32. Singhal M, et al. Synthesis of ZnO nanoparticles for varistor application using Zn-substituted aerosol OT microemulsion. Mater Res Bull 1997;32:239-247.

33. Dem'Yanets LN, et al. Zinc oxide: Hydrothermal growth of nano- and bulk crystals and their luminescent properties. J Mater Sci 2006;41:1439-1444.

34. Ristić M, et al. Sol-gel synthesis and characterization of nanocrystalline ZnO powders. J Alloy Comp 2005;39:L1-L4.

35. Wang Y, et al. Preparation of nanocrystalline metal oxide powders with the surfactant-mediated method. Inorg Chem Commun 2002;5:751-755.

36. Lu CH and Yeh CH. Emulsion precipitation of submicron zinc oxide powder. Mater Lett 1997;33:129-132.

37. Li X, et al. Synthesis and morphology control of ZnO nanostructures in microemulsions. J Colloid Interf Sci 2009;333:465-473.

38. Wei XQ, et al. Comparative study on structural and optical properties of ZnO thin films prepared by PLD using ZnO powder target and ceramic target. Opt Laser Technol 2009;41:530-534.

39. Schneider JJ, et al. Synthesis, characterization, defect chemistry, and FET properties of microwave-derived nanoscaled zinc oxide. Chem Mater 2010;22:2203-2212.

40. Yue S, et al. Synthesis of zinc oxide nanotubes within ultrathin anodic aluminum oxide membrane by sol-gel method. Mater Lett 2013;98:246-249.

41. Musić S, et al. Precipitation of ZnO particles and their properties. Mater Lett 2005;59:2388-2393.

42. Kabra V, et al. Low cost, p-ZnO/n-Si, rectifying, Nano heterojunction diode: Fabrication and electrical characterization. Beilstein J Nanotechnol 2014;5:2216-2222.

43. Xu J, et al. Grain size control and gas sensing properties of ZnO gas sensor. Sens Actuators B Chem 2000;66:277-279.

44. Zeng YJ, et al. Study on the Hall-effect and photoluminescence of N-doped p-type ZnO thin films. Mater Lett 2007;61:41-44.

45. Deng Q, et al. Ag nanoparticle decorated nanoporous ZnO microrods and their enhanced photocatalytic activities. ACS Appl Mater Interf 2012;4:6030-6037.